TRR
JOURNAL OF THE TRANSPORTATION RESEARCH BOARD

Research Article

Transportation Research Record
2023, Vol. 2677(3) 458–473

DOI: 10.1177/03611981221115729
journals.sagepub.com/home/trr
SAGE

Application of Unmanned Aerial Vehicles for Monitoring Airport Asset Surfaces

Surya Sarat Chandra Congress[1], Anand J. Puppala[2], Clayton Treybig[3], Charles Gurganus[3], and Jim Halley[4]

Abstract

Airports facilitate the fastest mode of transportation and connect local communities and businesses with national and international destinations. The American Society of Civil Engineers (ASCE) 2021 infrastructure report card rated the aviation infrastructure category with a D+. This highlights the need for frequent monitoring and performing timely preservation techniques to ensure the optimal performance of the asset. The Texas Department of Transportation (TxDOT) periodically inspects the regional airports in Texas through visual surveys and estimates the pavement condition index (PCI) for each airport on a network scale. These ratings are used to assess the need for rehabilitation in a timely manner. In this study, an attempt was made to use an unmanned aerial vehicle (UAV) mounted with an optical camera to inspect and evaluate the condition of various airport assets. Several observations were outlined to conduct a safe inspection of airport assets using UAVs. A comparison of PCI values, grouped into three categories, obtained from traditional and aerial inspections was made to understand the feasibility of using this new technology for airport asset management. It was observed that both inspections classified most of the airport assets similarly. The traditional inspection was observed to be quicker as it requires inspection of only sampled units, however, UAV data processing takes a relatively long time to offer a comprehensive digital footprint and immersive visualization experience of the whole airport assets. Overall, UAVs are identified to have a great potential as a data collection tool supplementary to the current traditional practices.

Keyword

transportation infrastructure, asset management, airport pavement, pavement condition index, small unmanned aerial vehicles, photogrammetry

Airports connect local communities and businesses to national and international destinations. They are classified based on access to the public and the type of activity. Depending on the activity, the airport assets experience different traffic loads and deteriorate over time. The recently released 2021 American Society of Civil Engineers (ASCE) infrastructure report card highlighted the sound condition of airport runways across the United States but rated the overall aviation infrastructure with a D+, which highlights the need for managing all airport assets in sound condition (*1*). Maintaining the condition of airport assets is key to improving the public's travel experiences. Airports with assets in poor condition can suffer from economic losses from the limitations levied on the operating loads of aircraft to ensure the safety of the air traffic. Monitoring and maintaining paved surfaces are among the most challenging tasks that aviation agencies face.

Federal and state agencies support the airport agencies to maintain optimum performance of the airport assets and provide good service to the general public.

[1]Department of Civil, Construction and Environmental Engineering, North Dakota State University, Fargo, ND
[2]Zachry Department of Civil and Environmental Engineering, Texas A&M Engineering Institute (TTI), Texas A&M University, College Station, TX
[3]Texas A&M Engineering Institute (TTI), Texas A&M University, Bryan, TX
[4]Airport Planning and Programming, Texas Department of Transportation, Austin, TX
[*]Surya Sarat Chandra Congress is also affiliated to Zachry Department of Civil and Environmental Engineering, Texas A&M Engineering Institute (TTI), Texas A&M University, College Station, TX; Texas A&M Engineering Institute (TTI), Texas A&M University, Bryan, TX and Anand J. Puppala is also now affiliated to Texas A&M Engineering Institute (TTI), Texas A&M University, Bryan, TX

Corresponding Author:
Anand J. Puppala, anandp@tamu.edu

The Texas Department of Transportation's (TxDOT's) Aviation Division collaborated with Texas A&M Transportation Institute (TTI) to inspect the airports in Texas periodically on a network level. Throughout the year, an airport surface inspector coordinates with the airport managers and conducts a traditional inspection to rate the airport asset surfaces. A condition assessment report for each airport is prepared to identify and prioritize the preservation/rehabilitation projects in the network. These reports are also used as a repository for planning the subsequent inspections at each of those airports. The reports are subjective to the experience of inspectors and denote the conditions of the representative sample units.

The advancement in building lightweight aerial platforms and compact sensors led to the recent revolution in the use of unmanned aerial vehicles (UAVs) for infrastructure monitoring applications. UAVs are being equipped with different sensors including visible, infrared, multi-spectral, and hyperspectral cameras, and light detection and ranging (LIDAR) for infrastructure inspections. The combination of UAV mounted with optical sensors, offering ease of data processing and affordability, is the most commonly used inspection tool in recent times. Photogrammetry is the science that uses two or more images for making remote measurements. Close-range photogrammetry by UAV (UAV-CRP) technology is widely being used to map infrastructure areas and assess the condition of assets (*2–7*). This study aimed to evaluate the application of UAV-CRP technology for mapping and assessing the conditions of the assets at a non-towered regional airport in Texas. A comparison between traditional inspections and UAV inspections was made to evaluate the feasibility of using the aerial data collection platforms.

This paper is organized as follows: the first section discusses various concepts pertinent to airport asset management, factors influencing pavement condition index (PCI), traditional inspection practices, and UAV applications. The subsequent section discusses the details of the regional airport and the data collection procedures adopted during the inspections. A few visuals that are representative of the condition of those assets are provided to give an idea about the quantitative inspections. PCI values calculated based on the condition assessments of assets obtained from both inspection methodologies were compiled and compared using the disagreement percentage. A discussion is provided to explore the potential reasons contributing to the differences between traditional inspection and unmanned aerial inspection. Various factors contributing to the difference in condition assessments are discussed. The final section concludes with the findings and recommendations about the potential application of these cutting-edge aerial sensor technologies.

Background

Airport Asset Management

Airfield pavement surfaces are subjected to varied traffic and environmental loadings that contribute to their deterioration. Pavement surface distress is inevitable, but proactive maintenance and preservation are expected to prolong the pavement's service life. In Texas, airports eligible to receive state funding are required to participate in the Texas Department of Transportation Aviation Division's Routine Airport Maintenance Program (RAMP). This is in addition to the already existing federal requirement for having a pavement management program for airports to be eligible for federal funding. RAMP is a cost-share program that has been in effect since 1996 and is effective in managing safe, serviceable, and durable airport pavement surfaces in the State of Texas.

Under this program, on request, a maximum of $50,000 is allocated annually from state funds, based on a 50/50 match by local funds. The funds can be utilized for various maintenance and improvement tasks that meet TxDOT's eligibility criteria (*8*, *9*). Efficient asset management is one of the objectives of the program, and airside improvements are preferred over landside tasks. Asset management can be accomplished through an efficient pavement management system that provides the condition of the pavement and predicts its remaining life span. It also estimates the time and resources needed to improve the condition of the asset and meet optimum performance standards.

During the first few years after construction, the curve depicting the relationship between the asset condition and time generally has a gentler slope. There is an optimum point in the asset life cycle graph after which the cost of renovation/rehabilitation increases exponentially. It is necessary to delay reaching that point by performing regular monitoring and timely preservation techniques. The Federal Aviation Administration (FAA) developed a manual that contains a set of guidelines and a simplified rating system to assist airport inspectors in rating the conditions of asphalt airfield surfaces (*10–12*).

Asset Condition Life Cycle

PCI rating is a numerical rating of the present pavement condition that ranges from zero to 100, with zero being the worst and 100 being the best possible condition, based on the extent and severity of various distress (*11*). It can neither measure the structural capacity nor provide a direct measurement of skid resistance or roughness. However, continuous monitoring of PCI provides an objective and rational basis for determining

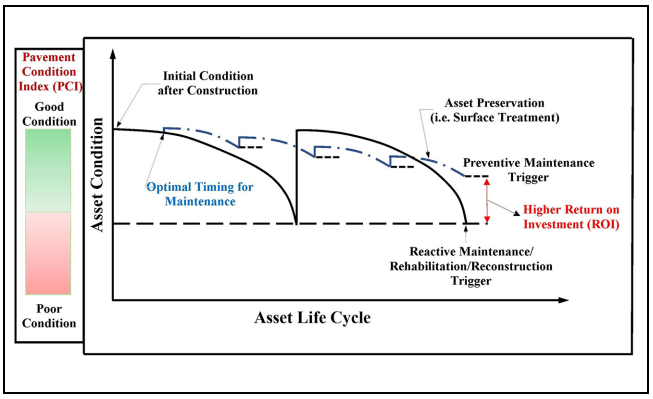

Figure 1. Airport asset condition life cycle.

maintenance and prioritizing repair needs. It can be plotted on the condition life cycle of an airport asset as shown in Figure 1, created and modified from the literature (*12*). Based on the condition and the life of the asset, optimal rehabilitation timing can be identified and performed to ensure a higher return on the investment, as can be observed from the difference between the rightmost ends of the last blue curve (dotted) and the black curve (solid). The blue and black curves represent preventive and reactive maintenance curves, respectively, of an airport asset. The difference between the asset condition at the end of the two curves, from preventive maintenance, indicates the longer life of the assets and reduced life cycle costs, which result in a higher return on investment. This also helps in the effective management, prioritization, and allocation of available funds to address the most critical areas. The condition assessments combined with economic analysis will provide airport agencies with sufficient information to set up short- and long-term plans for the available and expected funds (*10*).

Factors Influencing PCI

It should be noted that different distresses occur on different airport surfaces with various factors such as loading, environmental factors, construction deficiencies, or a combination thereof (*11*). The factors contributing to the occurrence of cracking along the centerline of a runway can be different from factors causing cracking at runway edges. The factors contributing to distress are classified into four categories: load, climate, construction, and others. Various types of distress falling under each contributing factor for asphalt and concrete surfaces are provided in Table 1.

When the PCI is very low, not only are the treatments expensive but they also take more time to complete. It is therefore advisable to reconstruct the section to gain more benefit for each dollar spent. Regular monitoring of pavement surfaces and assessing the conditions help in planning preservation techniques and preventing the pavement surfaces from deteriorating quickly (Figure 1). This also helps in reducing the financial losses arising from the downtime of the airport asset during any repair/rehabilitation tasks.

Traditional Practices

Preparation. Airport pavements are inspected and managed at a network level using FAA Condition Survey AC (150/5380-7B) and ASTM Standard D5340. First, the airport inspector prepares a map of the airport using data available on Google Earth and tools available in AutoCAD. A "Branch ID" is assigned to each airport for easy identification among hundreds of airports. The paved sections of the airport assets are classified based on their purpose and time of construction/work received and are assigned "Section IDs." Depending on the width of the runway, it is typically split into two sections along its transverse direction: runway edge and runway center. This classification is made because of the difference in the amount of loading received by the edge and center for wider runways. The central regions of the runways are highly trafficked and undergo load-related distress, whereas edge regions deteriorate from vegetation encroachment, poor drainage, and tractor/mower damage. Most of the other airport areas are recognized and classified by their purpose. Each section is also classified as "AC" or "PCC" based on the asphalt or concrete surface type, respectively. This is important since the condition evaluation of asphalt and concrete surfaces differ from each other (Table 1).

The previous works conducted at each of the airport's assets are tabulated to gain a better understanding of the existing conditions and contributing factors (Table 2). TxDOT's airport database, called Texas Airport Data System (TADS), acts as a repository of this information. Crack seals, patching, coal tar seals, fog seals, slurry seals, cape seals, mill and overlays, and reconstruction are some of the common works conducted based on the distress condition and location. If necessary, the occurrence of new work, reported in the database, is cross-checked by accessing the historical imagery on the Google Earth web platform. The length, width, and area of each section are accessed from the previous airport records. Each paved surface is ranked as primary, secondary, or tertiary based on the traffic or the importance of the pavement surface. Finally, a short description of where the pavement is located is also listed along with the above information to prepare a complete inventory inspection sheet for each airport before the inspection.

Sample Units. Typical airport inspection sheets contain the airport assets, work history, and blank spaces for

Table 1. Factors Contributing to Distress on Airport Surfaces

Contributing factors	Distress types	
	Asphalt surfaces	Concrete surfaces
Load	Alligator cracking and rutting	Corner break, LTD cracking, pumping, and shattered slab
Climate	Block cracking, joint reflection cracking, LT cracking, raveling, shoving, and weathering	Blowup, durability cracking, joint seal damage, and pop-outs
Construction	Bleeding, corrugation, depression, polished aggregate, slippage cracking, and swelling	Alkali-silica reaction, scaling, and shrinkage cracking
Others	Jet blast erosion, oil spillage, and patching and utility cut patching	Corner spalling, joint spalling, settlement or faulting, small patching, and large patching/ utility patch

Note: LT = Longitudinal and Transverse; LTD = Longitudinal, Transverse, and Diagonal.

Table 2. Construction and Preservation Work Details of Each Airport Asset

Section	Construction	Preservation techniques performed		
		Work1	Work2	Work3
Runways				
R 04-22	4/1/1983	Slurry seal 7/1/1993	Coal tar seal 4/26/2005	
R 17-35	7/1/1990	Coal tar seal 9/1/1999	Overlay 7/1/2008	Coal tar seal 8/1/2015
Taxiways				
T-A 04 17	7/1/1993	Coal tar seal 9/1/1999	Fog 03/20/2012	
T-A 17	7/1/1993	Coal tar seal 9/1/1999	Fog 03/20/2012	
T-A Main	7/1/1974	Coal tar seal 9/1/1999	Fog 03/20/2012	
T-B	7/1/2012			
T-C	7/1/1993	Coal tar seal 9/1/1999	Fog 03/20/2012	
T-D	7/1/1993	Coal tar seal 9/1/1999	Fog 03/20/2012	
T-E	5/1/2008			
Helipads				
A-Heli 1	8/1/2015			
A-Heli 2	8/1/2015			
A-Heli 3	8/1/2015			
Aprons				
A-Main	7/1/1993	Coal tar seal 9/1/1999	Fog 03/20/2012	Overlay 10/1/2019
A-Park	8/1/2015	Coal tar seal 8/2/2015		
A-West	11/1/2001			
A-17	7/1/1993	Coal tar seal 9/1/1999	Fog 03/20/2012	

Note: White (empty) cells represent no work details to report.

quick marking of the asset conditions. These inspections are not used for project analysis but are used to manage at a network level. The chart in the ASTM Standard D5340 is used for determining the number of sample units for each asset. Though the ASTM Standard specified the inspection of 10% of sample units, at least 20% of the total sample units of each airport asset considered in the current study were inspected. To be efficient, the amount and size of sample units are marked on the sheets before conducting the actual inspection. Sufficient measures are followed to have a sample size and extent that is easy to identify during the inspection. For example, the existing markings and their approximate lengths are used while identifying these sample units during the actual inspection. It should be noted that there are some differences between rating an asphalt surface and a concrete surface because of the differences in the types of their distresses.

The typical practice uses a sample unit size of 5,000 ft^2 $\pm$ 2,000 ft^2 (464.5 m^2 $\pm$ 185.8 m^2) for each of the asphalt surfaces. They are adjusted in shape, as needed, to inspect accurately and efficiently. For example, some

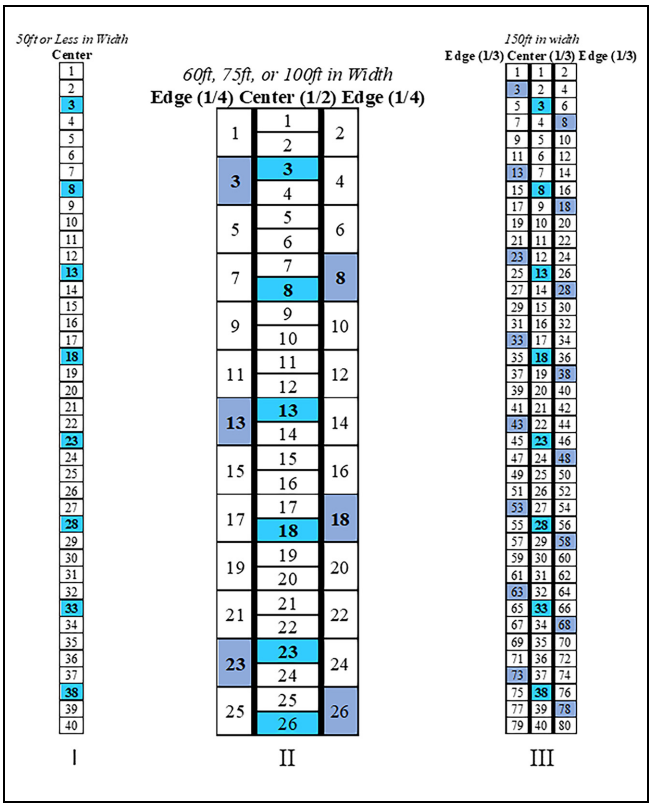

Figure 2. Allocation of sample units for inspection of the airport assets.

taxiways are 35 ft (10.7 m) wide, so 150 ft (45.7 m) long sections of the taxiway will be rated to inspect every 5,250 ft^2 (487.7 m^2) surface area of the asset. The concrete pavement surfaces are rated slab by slab. The typical inspection practice for concrete pavements uses a sample unit size of 20 slabs ± 8 slabs that are adjacent to each other. This is also adjusted based on the widths of pavement sections for accuracy and efficiency. If there are multiple instances of the same distress on a concrete slab, only the distress with higher severity is counted.

Generally, these sample units are selected randomly and spread out as per the ASTM Standard to collect representative data of the entire section. Sometimes 20% or more of the asset surface area is inspected because of the size of the pavement section. For example, ladder taxiways and turn-around aprons near the end of a runway have low surface area. In these cases, there might be only one or two total sample units, resulting in a 50% or 100% inspection of those surfaces. An "additional sample unit" is created on the inspection sheet if the inspector identifies a unique area with distress that is not representative of the whole section. This sample unit is used to estimate the condition ratings but with a different weightage to avoid bias in the inspection assessments. Figure 2 shows the criteria used for selecting the sample units for inspecting the airport asset surfaces using both traditional and UAV methods in this study.

Sampling information for three types of runways, classified by width, having a length of 4,000 ft (1,219 m) is provided as follows. In Case I, where the width of the runway is less than or equal to 50 ft (15 m), a 4,000 ft (1,219 m) long runway may have a maximum surface area of 200,000 ft^2 (18,580 m^2). A maximum total of 40 sample units, with a sample unit size of 5,000 ft^2 (465 m^2) spanning around 100 ft (30.5 m) long over the full width of the runway can be considered. At least eight sample units need to be inspected to obtain a minimum of 20% representative condition assessments.

Case II shows a runway having a width greater than 50 ft (15 m) and less than 100 ft (30.5 m). A 4,000 ft (1,219.2 m) long and 75 ft (22.9 m) wide runway may have a maximum surface area of 300,000 ft^2 (27,870.9 m^2) divided equally into the center and edge regions, as shown in Figure 2. A maximum total of 26 sample units each for the center and edge regions can be considered. For the runway center, a sample unit size of 5,625 ft^2 (523 m^2) spanning over 150 ft (46 m) length of the central region of the runway having a width of 37.5 ft (11 m) can be considered. For the runway edge regions on either side, a sample unit size of 5,625 ft^2 (523 m^2) spanning over 300 ft (91 m) length of the edge regions of the runway having a width of 18.75 ft (5.7 m) can be considered. At least six sample units need to be inspected each for the center and edge regions to obtain a minimum of 20% representative condition assessments.

A runway 4,000 ft (1,219 m) long and 150 ft (46 m) wide in Case III may have a maximum surface area of 600,000 ft^2 (55,742 m^2). The surface area is divided equally into three parts, as shown in Figure 2. For the runway center, a maximum total of 40 sample units with a size of 5,000 ft^2 (465 m^2) spanning over 100 ft (30.5 m) length of the central region of the runway having a width of 50 ft (15 m) can be considered. For the runway edge regions on either side, a maximum total of 80 sample units having a size of 5,000 ft^2 (465 m^2) spanning over 100 ft (30.5 m) length of the edge regions of the runway having a width of 50 ft (15 m) can be considered. The sample units inspected in the central and edge regions of the runway are marked in aqua and blue, respectively, as shown in Figure 2. A similar methodology was adopted to arrive at the sample units for all airport assets inspected using traditional and UAV-based methods.

Data Collection. The visual inspections of runways, taxiways, helipads, and aprons are supplemented with pictures, videos with and without narration, deflection testing, and profile testing. The profile run of the runway is conducted along the centerline by placing a camera on top of the inspection vehicle to capture video and narrate

the conditions of the runway. This high-speed run is also used to provide a cursory evaluation of runway smoothness. Sometimes a mobile application is also used as a basic screening tool to give an idea of the runway smoothness/roughness and evaluate the need for performing actual profiler studies at the airport. An inertial profiler provides the input data required for conducting an FAA Boeing Bump Index analysis of the runway smoothness. The FAA Boeing Bump Index format currently classifies the condition into three types: good (green), fair (yellow), and poor (red).

In most cases, a lightweight deflectometer (LWD) is also used to get an idea of the strength of pavement surfaces near the runway ends, the hold short lines of major taxiways, and on the main parking aprons, which receive heavier loads from the movements of airplanes with full fuel capacity. As part of these tests, a laser thermometer is used to measure the pavement temperature and a 10 kg weight is dropped three times to measure the average modulus. At each runway end, this test is conducted at 1.8 m (6 ft) on both sides of the centerline and also on the centerline. This is performed as a screening test to evaluate the need for conducting a falling weight deflectometer test and analysis. According to AC150/5370-11B, a project-level FAA evaluation requires approximately 150 to 250 deflection tests on a runway (*13*). This testing is intended to provide a relative indication of the pavement strength and make qualitative assessments about the appropriate aircraft loading.

Unmanned Aerial Vehicles (UAVs)

Today's widespread use of UAVs for infrastructure applications in the United States can be traced back to the early contributions made by the U.S. military and the National Aeronautics and Space Administration (NASA) toward the development of robust and reliable unmanned aerial platforms for reconnaissance applications. The past few decades have witnessed a phenomenal rise in the development of compact high-capacity sensors at an affordable cost. These advancements coincided with the improvement in the computational power of the systems and readily available image processing algorithms. In 2016, FAA released the initial safe operation guidelines for the commercial use of UAVs. Over the years, FAA has been proactively initiating programs such as Low Altitude Authorization and Notification Capability (LAANC), UAS Integration Pilot Program (IPP), and so forth, for the safe operation and integration of UAVs into the nation's airspace.

In 2021, FAA released an additional set of rules covering various topics including UAV categories, remote ID, and many other safety guidelines. All these factors were instrumental in the application of UAVs for various civil infrastructure applications. A few of the applications of UAVs include monitoring traffic patterns, crash scenes, avalanches, disaster response, pavements, airports, bridges, rail corridors, dams, embankments, spillways, towers, and many other structures (*14–24*). Only a few studies have been conducted on using UAVs for airport inspections (*25*, *26*). One of the recent studies was funded by the Airport Cooperative Research Program, which proposed various applications of UAVs for airport inspections on a general level (*26*). Several other studies on the type of platforms and the flight characteristics for collecting airport asset condition data using UAVs are being conducted.

Conducting in-depth pavement surface inspection of airport assets using UAVs poses many challenges, partly contributed to by the challenging nature of the airspace at airports and also the relative newness of the technology. The authors of the current study conducted a UAV-based inspection of various civil engineering-related structures including pavements, non-operational airport runways, bridges, rail corridors, dams, embankments, spillways, towers, and buildings using visible and infrared sensors. Semi-automated machine learning techniques were also used to segregate aerial imagery and evaluate infrastructure conditions (*27*). The experience in conducting all the above inspections helped the authors collaborate with TxDOT to plan and conduct the UAV-based inspection of a non-towered regional airport without closing it to air traffic. The conservative and safest option would have been to close the runway during the unmanned aerial inspections; however, the authors planned and executed the data collection tasks in such a way as to avoid any inconvenience to the airport users and demonstrate the flexibility and safety of using these cutting-edge aerial technologies.

Airport Case Study

Asset Details

A public non-towered airport, with two runways, seven taxiways, three helipads, and many apron areas, was inspected by both traditional and aerial methods to assess the condition of its assets. The construction dates and the subsequent preservation work details are provided in Table 2. Runway 17-35 is longer and wider than Runway 04-22, which is a relatively old runway and has poor markings. Runway 17-35 is aligned in the north–south direction and Runway 04-22 is aligned in the southeast direction of the first runway, with runway end 04 beginning adjacent to the 35 end of the first runway.

The seven taxiways are: T A 17, T B, T C, T D, T E, T A 04-17, and T A Main. Taxiways A Main and E connect the landside areas to the airside assets. Taxiway D runs parallel to R 04-22 and joins the T A Main and Runway

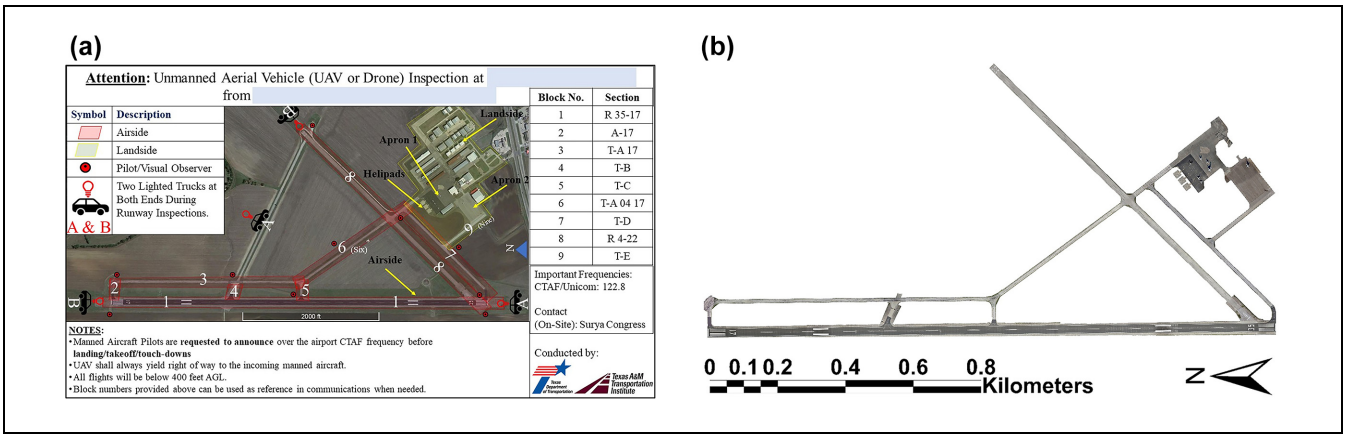

Figure 3. Unmanned aerial vehicle inspection of airport assets: (*a*) typical flight mission advertisement for notifying airport users about unmanned aerial inspections, and (*b*) visualization of airport assets using unmanned aerial data analysis.

end 35 at its both ends. Taxiway A Main crosses Runway 04-22 and proceeds toward the airside areas as Taxiway A 04-17, which meets T A 17 and T C. Taxiway A 17 runs parallel to the main Runway 17-35 and is connected to R 17-35 by the two Taxiways B and C before curving in to join the main runway at the end 35, as shown in Figure 3. Three helipads, aligned parallel and adjacent to each other, are located north of Apron A-Park. There are many apron areas but only the condition assessments of the main areas such as the A- Park, A-Main, A-West, and A 17 are provided and discussed in the current study. Apron A 17 is located near the end 17 of the main runway and experiences many slow-moving and idling aircraft waiting before entering the main runway.

Data Collection

Traditional Inspections. All preparation steps described in the above section on traditional inspection were followed to prepare the inspection forms and conduct a PCI visual survey at the non-towered airport. To facilitate the comparison of inspections conducted with UAVs, an inspection vehicle was equipped with a global positioning system (GPS) to obtain location information of the inspected sample units and compare the assessments with UAV inspections.

UAV Inspections. The authors followed a framework to collect the aerial data using a UAV equipped with an optical camera. The average flight altitude above the airport assets was maintained at approximately 22 m. For the current study, the drone was assembled with an additional geographical navigation satellite system (GNSS) configuration. A ground base station was also used to obtain post-processed kinematic (PPK) GNSS information and accurately georeference the images.

The flight data collection tasks were divided into three stages: pre-flight, mission flight, and post-flight. The pre-flight tasks involved the planning of flights, coordination with Airport Operations and Safety Management System officers and other airport stakeholders, preliminary reconnaissance, seeking authorizations, and unlocking the drone. The airport manager was also provided with an advertisement brochure about the unmanned aerial inspections for circulation among the airport users (Figure 3*a*). Mission flight tasks involved the activities conducted on the day of data collection. The day started with the collection of ground point information followed by site reconnaissance to verify the feasibility of conducting planned flights. The inspections were conducted, during daylight only, with two lighted trucks stationed at both ends of the runways. The drone remote pilot in command (RPIC) listened to the common traffic advisory frequency (CTAF) and yielded to the manned aircraft by landing the drone and clearing off the runway.

The interruptions from aircraft maneuvers did increase the overall data collection time; however, this also highlights the flexibility of these aerial platforms to resume the data collection from the previous data collection point (waypoint) in the planned flight mission. After data collection, the post-flight stage involves a quality check, debriefing, geotagging, and sorting of the flight data. One of the benefits of the UAV-CRP technology is that it provides an option to check the quality of the data and area covered by building low-quality model for a quick review. This will reduce the inspection costs if the data collection tasks must be repeated at a later date because of poor quality/incomplete data.

Subsequently, the images were sorted into different flights under each airport asset and the geotagging information was corrected using PPK-GNSS information obtained from a combination of sensors and equipment.

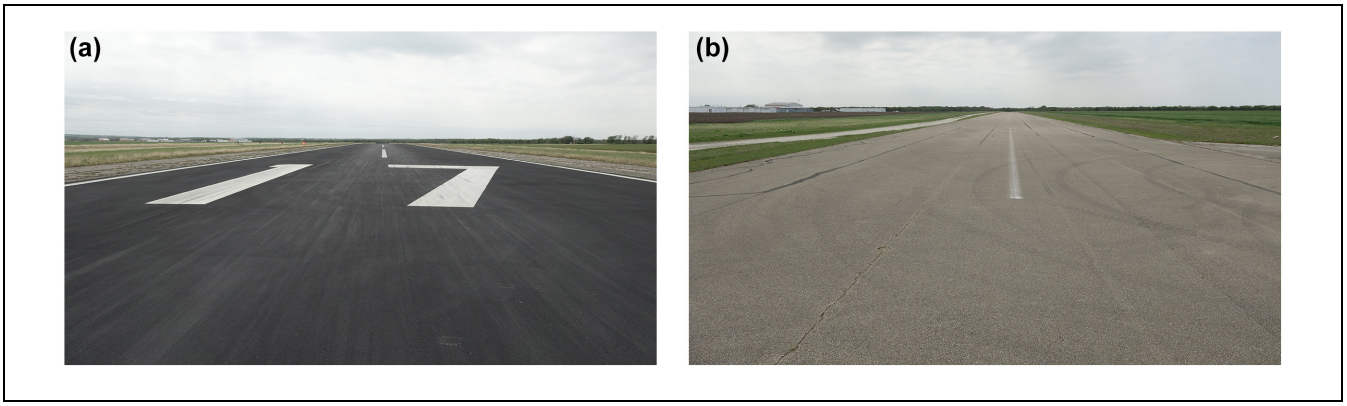

Figure 4. Traditional inspection of runways: (*a*) R 17-35 and (*b*) R 04-22.

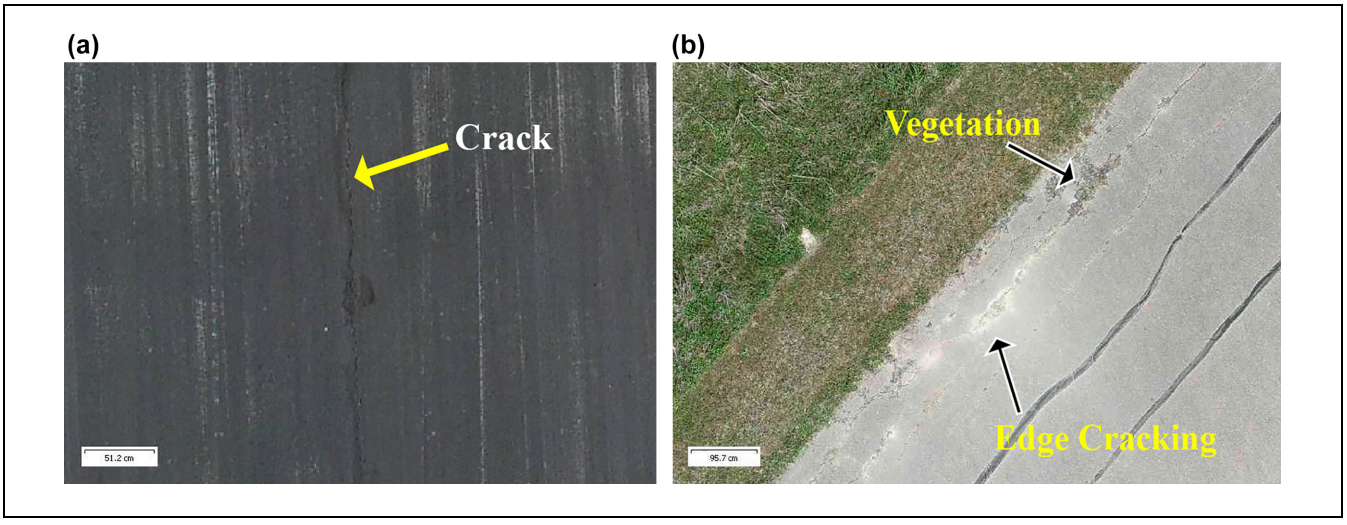

Figure 5. Aerial inspection of runways: (*a*) R 17-35 and (*b*) R 04-22.

These geotagged images were processed using photogrammetric software to develop three-dimensional (3D) mapping products for further analysis (*20*). The orthomosaic can be rendered on either the mesh or digital surface model to obtain an accurate scaled view. The scale in the orthomosaics of the airport assets inspected by the UAV-CRP technology can be observed in Figure 3*b*. These scaled images also facilitate making measurements of the distresses and condition assessments, discussed in the subsequent sections.

Condition Assessments

Condition assessments from both techniques were compared by synchronizing the GPS measurements collected during the traditional inspections with the locations in the georeferenced 3D models generated using the aerial images. Representative pictures of the conditions existing at various airport assets inspected by both traditional and aerial inspections are provided in Figures 4–11.

Runways

Traditional Inspection. It should be noted that during traditional inspections, images at selected locations and videos of high-speed runs along each airport asset were captured. The images of runways captured during the inspection by a traditional inspector are provided in Figure 4. Following the sampling techniques discussed, the R 04-22 and R 17-35 were divided similarly to Case I and Case II, respectively, for inspections.

The sum of the distresses on all sample units was calculated for both runways as follows. R 17-35 Center-1 exhibited 1,455 ft (443 m) of low severity cracking and 440 ft (134 m) of medium severity cracking. R 17-35 Edge-1 exhibited 154 ft (47 m) of low severity cracking and 27 ft (8 m) of medium severity cracking. R 04-22 exhibited (a) 3,580 ft (1,091 m) of low severity cracking,

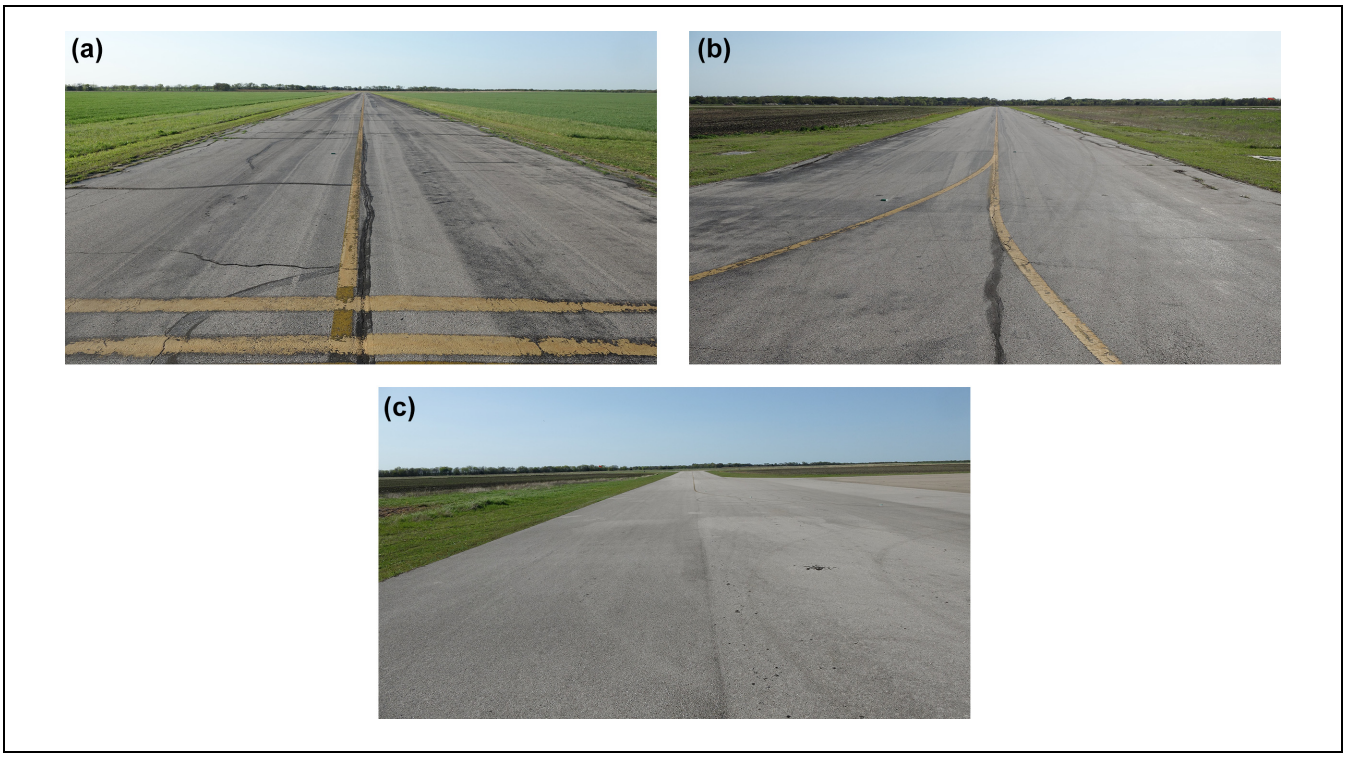

Figure 6. Traditional inspection of taxiways: (*a*) T-A 04 17, (*b*) T-D, and (*c*) T-E.

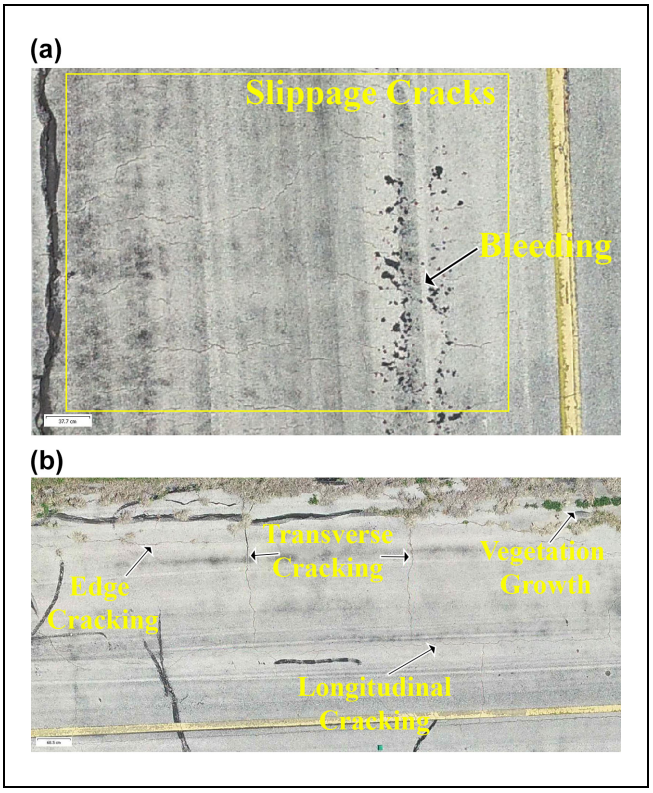

Figure 7. Aerial inspection of taxiways: (*a*) slippage cracks and bleeding on Taxiway A 17 and (*b*) distress on Taxiway C.

2,790 ft (850 m) of medium severity cracking, and 10 ft (3 m) of high severity cracking; (b) 400 ft^2 (37 m^2) of medium severity block cracking; and (c) 38,500 ft^2 (3,577 m^2) of medium severity weathering.

Aerial Inspection. An orthomosaic is a scaled image generated by stitching multiple images viewing the area of interest. The size of each pixel in the orthomosaic is equal to the ground sampling distance, which can be estimated based on the flight and sensor characteristics. The scale provided at the bottom left corner of the figures provides an idea about the extent of distress. Different distresses on both the runways were identified and measured from the orthomosaics, as shown in Figure 5.

The sum of the distresses on all sample units was calculated for both runways as follows: R 17-35 Center-1 exhibited 484 ft (148 m) of low severity cracking and 870 ft (265 m) of medium severity cracking. R 17-35 Edge-1 exhibited 136 ft (41 m) of low severity cracking and 45 ft (14 m) of medium severity cracking. R 04-22 exhibited (a) 3,690 ft (1,125 m) of low severity cracking and 604 ft (184 m) of medium severity cracking; (b) 2,257 ft^2 (210 m^2) of high raveling; and (c) 38,500 ft^2 (3,577 m^2) of low severity weathering.

Taxiways

Traditional Inspection. The condition of the Taxiways T-

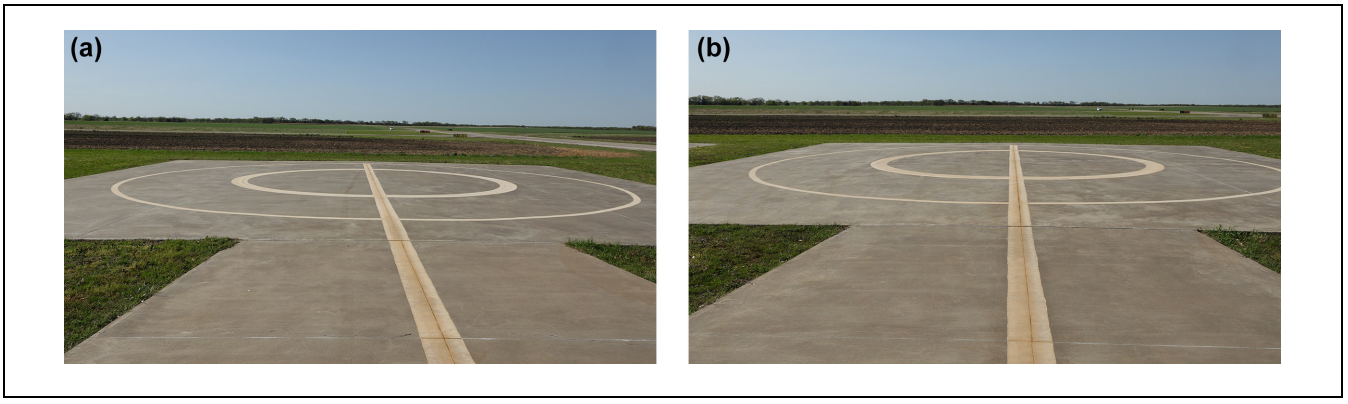

Figure 8. Traditional inspection of helipads: (*a*) Helipad 1 and (*b*) Helipad 2.

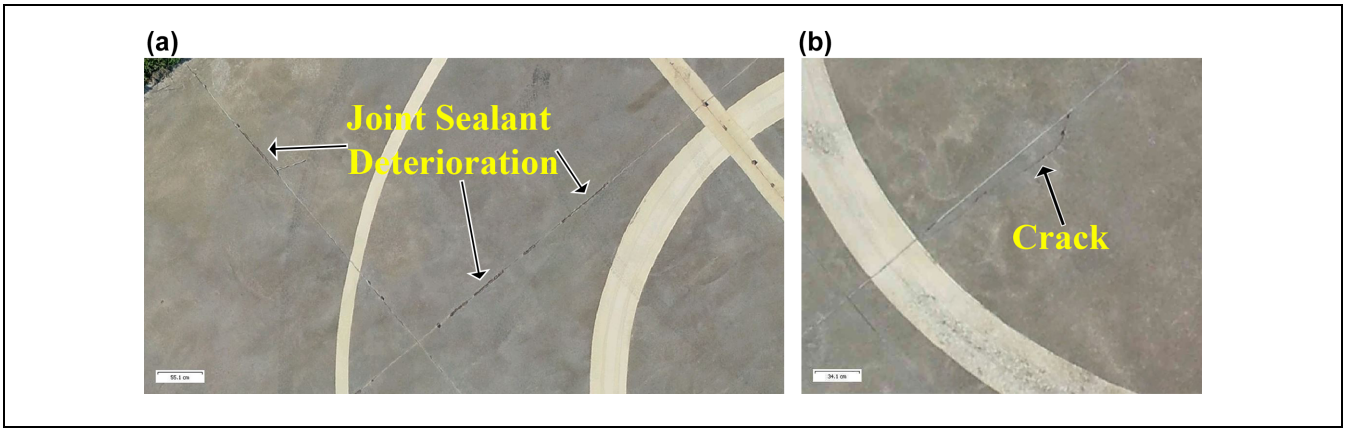

Figure 9. Aerial inspection of helipads: (*a*) joint sealant deterioration on Helipad 1 and (*b*) joint spalling on Helipad 3.

A 04 17, T-D, and T-E captured during the traditional inspection are provided in Figure 6. It can be observed that all three taxiway surfaces weathered significantly. There was bleeding on T-A 04 17 surface. Edge distress and vegetation encroachment can be observed on both T-A 04 17 and T-D surfaces.

The sum of the distresses on all sample units was calculated for seven taxiways as follows: T-A 17 exhibited 1,610 ft (491 m) of low severity cracking and 2,150 ft (655 m) of medium severity cracking. T-B exhibited (a) 10 ft (3 m) of low severity cracking and 55 ft (17 m) of medium severity cracking; and (b) 4,000 ft^2 (371 m^2) of low severity weathering. T-C exhibited (a) 715 ft (218 m) of low severity cracking and 700 ft (213 m) of medium severity cracking; and (b) 6,206 ft^2 (577 m^2) of low severity weathering. T-D exhibited (a) 1,070 ft (326 m) of low severity cracking, 1,080 ft (329 m) of medium severity cracking, and 370 ft (113 m) of high severity cracking; (b) 240 ft^2 (22 m^2) of slippage cracking, and (c) 15,750 ft^2 (1,463 m^2) of low severity weathering.

T-E exhibited (a) 15 ft (5 m) of low severity cracking; and (b) 10,500 ft^2 (975 m^2) of low severity weathering. T-A 04 17 exhibited (a) 490 ft (149 m) of low severity cracking, 1,170 ft (357 m) of medium severity cracking, and 20 ft (6 m) of high severity cracking; (b) 830 ft^2 (77 m^2) of bleeding; and (c) 10,500 ft^2 (975 m^2) of low severity weathering. T-A Main exhibited (a) 440 ft (134 m) of low severity cracking and 240 ft (73 m) of medium severity cracking; (b) 350 ft^2 (33 m^2) of slippage cracks; and (c) 5,000 ft^2 (465 m^2) of medium severity weathering.

Aerial Inspection. The conditions of the taxiway surfaces observed in the orthomosaics developed from the UAV data are provided in Figure 7. Different distresses, such as bleeding, longitudinal, transverse, edge, and slippage cracks, along with vegetation encroachment, can be observed in Figure 7. Slippage cracks were observed to be formed near the taxiway areas that experience slow-moving aircraft traffic in the course of runway crossing maneuvers. The 3D models developed from aerial two-dimensional imagery help in identifying the exact locations of these distress and provide scope to understand the potential cause of distress.

Figure 10. Traditional inspection of aprons: (*a*) Apron A-17, (*b*) Apron A-Main, and (*c*) Apron A-West.

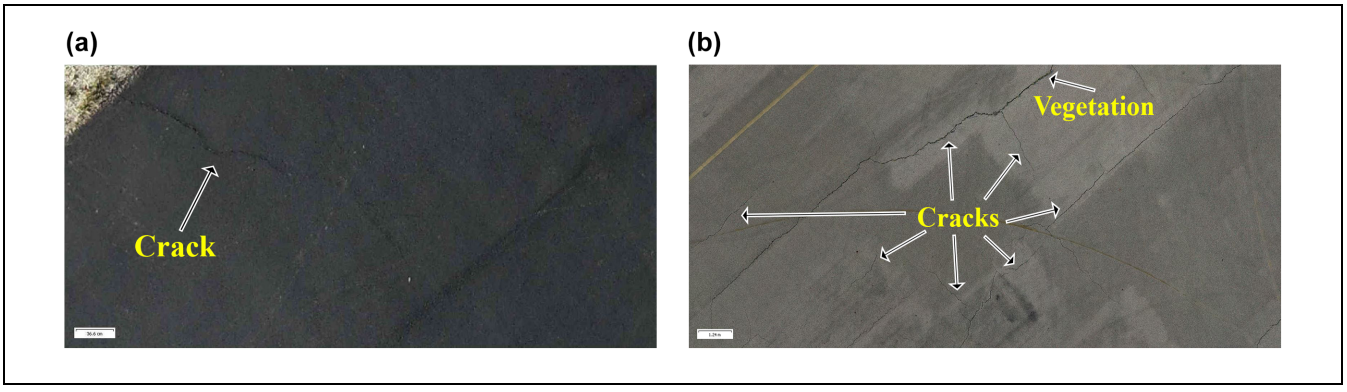

Figure 11. Aerial inspection of aprons: (*a*) Apron A-Park and (*b*) Apron A-West.

The sum of the distresses on all sample units was calculated for seven taxiways as follows: T-A 17 exhibited (a) 161 ft (49 m) of low severity cracking and 684 ft (209 m) of medium severity cracking; (b) 2,274 ft^2 (211 m^2) of bleeding; (c) 3,340 ft^2 (310 m^2) of high severity raveling; (d) 506 ft^2 (47 m^2) of slippage cracks; and (e) 21,000 ft^2 (1951 m^2) of low severity weathering. T-B exhibited 43 ft (13 m) of low severity cracking and 110 ft (33 m) of medium severity cracking; (b) 2 ft^2 (0.15 m^2) of medium severity raveling; and (c) 4,000 ft^2 (372 m^2) of low severity weathering. T-C exhibited (a) 217 ft (66 m) of low severity cracking and 423 ft (129 m) of medium severity cracking; (b) 2038 ft^2 (189 m^2) of high severity raveling; and (c) 6,206 ft^2 (577 m^2) of low severity weathering. T-D exhibited (a) 286 ft (87 m) of low severity cracking and 398 ft (121 m) of medium severity cracking; (b) 2,191 ft^2 (204 m^2) of high severity raveling; (c) 869 ft^2 (81 m^2) of slippage cracking; and (d) 15,750 ft^2 (1,463 m^2) of low severity weathering.

T-E exhibited (a) 10 ft (3 m) of low severity cracking; and (b) 10,500 ft^2 (975 m^2) of low severity weathering. T-A 04 17 exhibited (a) 367 ft (112 m) of low severity cracking and 198 ft (60 m) of medium severity cracking; (b) 572 ft^2 (53 m^2) of bleeding; (c) 1,133 ft^2 (105 m^2) of high

severity raveling; and (d) 10,500 ft^2 (975 m^2) of low severity weathering. T-A Main exhibited (a) 583 ft (178 m) of low severity cracking and 56 ft (17 m) of medium severity cracking; (b) 1,864 ft^2 (173 m^2) of slippage cracks; and (c) 10,000 ft^2 (930 m^2) of low severity weathering.

Helipads

Traditional Inspection. The helipads were constructed with concrete slabs, as shown in Figure 8. Concrete surfaces are inspected for different types and extents of distress compared with asphalt surfaces. Generally, in addition to the type of distress, it is also necessary to identify the number of slabs affected by the distress rather than the length of distress as measured in the case of asphalt surfaces.

The sum of the distresses on all sample units was calculated for the three helipads as follows. Helipad 1 exhibited (a) one slab with low severity corner break; and (b) two slabs with low severity cracking. Helipad 2 exhibited no distress. Helipad 3 exhibited (a) one slab with shrinkage cracking; and (b) one slab with a low severity joint spall.

Aerial Inspection. The high-resolution images used to generate the 3D models helped in identifying the joint sealant deterioration on Helipad 1, as shown in Figure 9. This is important to identify as proper sealant prevents moisture intrusion and subsequent concrete slab failures caused by loss of support. Joint spalling distress is also observed on Helipad 3 (Figure 9).

The sum of the distresses on all sample units was calculated for three helipads as follows. Helipad 1 had (a) three slabs with low severity linear cracking; and (b) 20 slabs with low severity joint sealant damage. Helipad 2 exhibited no distress. Helipad 3 had one slab with a low severity joint spall.

Aprons

Traditional Inspection. The condition of the aprons captured during traditional inspection can be observed in Figure 10. Apron A-17 experiences aircraft traffic idling before entering the main Runway 17-35. Aprons A-Main and A-West were commonly used for parking the aircraft. Apron A-West can be observed to exhibit multiple cracks on the surface, as shown in Figure 10.

The sum of the distresses on all sample units was calculated for four aprons as follows. A-Park exhibited 55 ft (17 m) of low severity cracking. A-Main exhibited (a) 10 ft (3 m) of low severity cracking; and (b) 22,500 ft^2 (2,090 m^2) of low severity weathering. A-West exhibited (a) 600 ft (183 m) of low severity cracking and 910 ft (277 m) of medium severity cracking; and (b) 19,500 ft^2 (1,812 m^2) of high severity weathering. A-17 exhibited (a) 280 ft (85 m) of low severity cracking; (b) 675 ft^2 (63 m^2) of bleeding; and (c) 5,454 ft^2 (507 m^2) of medium severity weathering.

Aerial Inspection. Apron A-Park is observed to have only minor distress, as shown in Figure 11. However, there are multiple cracks on the Apron A-West. There are traces of vegetation growing through these cracks, as shown in Figure 11.

The sum of the distresses on all sample units was calculated for four aprons as follows. A-Park exhibited 19 ft (6 m) of low severity cracking and 23 ft (7 m) of medium severity cracking. A-Main exhibited (a) 20 ft (6 m) of medium severity cracking; (b) 22,500 ft^2 (2,090 m^2) of low severity weathering; and (c) 26 ft^2 (2 m^2) of oil spillage. A-West exhibited (a) 127 ft (39 m) of low severity cracking and 2,230 ft (680 m) of medium severity cracking; and (b) 19,500 ft^2 (1,812 m^2) of medium severity weathering. A-17 exhibited (a) 75 ft (23 m) of medium severity cracking; (b) 1,548 ft^2 (144 m^2) of bleeding; (c) 5,454 ft^2 (507 m^2) of medium severity weathering; and (d) 2,727 ft^2 (254 m^2) of oil spillage.

Traditional inspection, when conducted stationarily, offers a close-up view of only the sampled surfaces and the ability to feel the surface, if necessary. One of the advantages of UAV-based photogrammetric mapping is its ability to provide scaled views and measurements of the whole of the airport assets from remotely collected data. This can be observed in all the aerial inspection images, notably in Figure 7*b* which also provides an idea about the proximity of the vegetation encroachment to the centerline of the taxiway. The dimensions of the distress, which are mostly obtained through visual inspections in traditional practices, can be obtained precisely by multiplying the number of pixels occupied by the distress with the resolution of the orthomosaics developed from aerial images. This helps to classify the distress severity levels and measure the extent to estimate the PCI without introducing subjectivity from the experience of the inspector, as in the case of traditional inspections.

Pavement Condition Index (PCI) Assessment

Based on the distress assessments made in the above sections, the PCI of each asset was estimated by inputting the extent of the distress in Paver software. The Paver software has input options for various distresses and their severities to deduct the values and calculate PCI. Further, the PCI values of the inspected sample units are extrapolated to obtain a representative PCI value of the whole airport asset surface. Based on the PCI values obtained for each asset, the condition of each asset was indicated by the respective colors shown in Figure 12 (*11*).

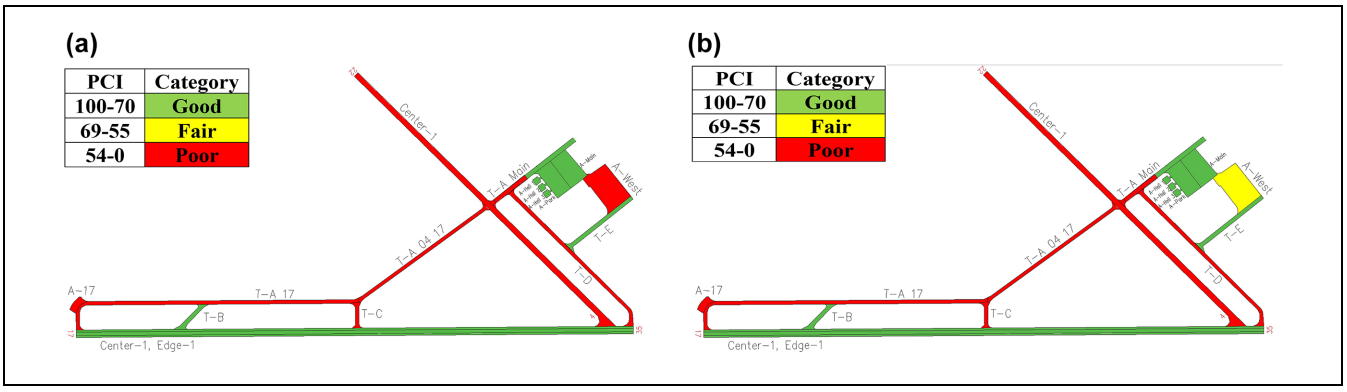

Figure 12. Pavement condition indices (PCIs) of airport assets obtained from: (*a*) traditional inspection and (*b*) unmanned aerial vehicle inspection.

Paver software stores the condition assessment data and also serves as a repository of inspections conducted at different airports during different time periods. Table 3 provides a comparison of the PCIs for each asset from both inspections, contributing factors for deducting PCI values, and the disagreement percentage. The difference between both PCI values of each asset was divided by the PCI of traditional inspection and expressed as the disagreement percentage.

Discussion

The condition of the assets was observed to be influenced by the date of construction and the type of most recent maintenance activity performed (Table 2). It can be observed in Figure 12 that all the airport assets except for one, that is, Apron A-West, are similarly classified by both inspections. It should be noted that the wide range of PCI values in each condition category is one of the reasons for these similarities in Figure 12. However, comparisons between the PCI values and the respective disagreement percentages in Table 3 provide more insights into the differences in condition assessments.

The disagreement percentages of half of the assets inspected are within 10% (Table 3). All of these assets were classified as "good" by both inspection methods, as shown in Figure 12. This affirms the ability of UAV inspections to depict the existing conditions of "assets performing well" similar to the traditional inspections.

Although the rest of the assets, except Apron A-West, were classified under the same condition category by both inspection methods, the difference in PCI values can be observed from the disagreement percentages shown in Table 3. The disagreement percentage is higher for assets whose PCI values are influenced by the presence of cracks. UAV inspections were able to depict the existing conditions and identify higher extents of distress compared with traditional inspections conducted by visual observation. This can be attributed to the 3D models facilitating the accurate measurement of distress features in a digital environment compared with a traditional visual inspection in the field. Besides, the traditional inspections considered edge cracking as the number of feet of longitudinal and transverse cracks. It is difficult to account for all linear measurements of cracks near edge cracking regions because of the complexity created by the vegetation encroachment. Under UAV inspections, the edge cracking was considered as raveling and measured the area of distress for PCI calculations.

One other reason for the difference in PCI values obtained from both methods was that the traditional inspections considered the airport assets as medium and highly weathered surfaces. This was the main reason for the difference in the PCI values of Apron A-West. An in-person stationary visual survey offers the ability to view and feel the surface from a closer distance to inspect it at a granular level. However, given the vastness of the airport assets, the traditional visual survey cannot provide eyes on the whole airport assets and scaled views as is the case with the models developed from aerial imagery. Although it is possible to collect the aerial data at a granular level, for the given UAV and camera specifications, by flying at a lower flight altitude, it may not be practical and efficient to perform such assessments unless it is necessary for certain exceptional reasons or smaller areas. The data generated with such high resolution poses issues of data management and storage.

The aerial condition assessments were able to detect various distress such as bleeding, cracks, slippage cracks, vegetation growth, raveling, sealant deterioration, and shrinkage cracks. Moreover, UAV data can provide location information of each distress type which can be fed automatically into a GIS-based condition inventory database for asset management purposes. This also facilitates quick decision making by the stakeholders and timely response by the airport manager to prioritize and address the most critical distresses.

Table 3. Airport Infrastructure Asset Management

Asset name/ section ID	Pavement condition index (PCI) values		Contributing factors	Absolute disagreement percentage (%)
	Traditional inspection	Unmanned aerial vehicle inspection		
Runways				
R 17-35	83	81	Cracking at centerline	2
Center-1				
R 17-35	97	97	Normal performance	0
Edge-1				
R 04-22	54	45	Age, cracks, lack of treatment	17
Center-1				
Taxiways				
T A 17	35	22	Age, poor bond between layers, many wide cracks	37
T B	81	74	Lacks seal	9
T C	51	27	Age, many wide cracks	47
T D	43	24	Age, poor bond between layers, many wide cracks	44
T E	92	93	Lacks seal	1
T A 04-17	40	27	Age, surface bleeding, many wide cracks	33
T A Main	40	14	Age, poor bond between layers, many wide cracks	65
Helipads				
Helipad 1	92	87	Normal performance	5
Helipad 2	100	100	Normal performance	0
Helipad 3	97	98	Normal performance	1
Aprons				
A - Park	97	97	Normal performance	0
A - Main	93	91	Normal performance	2
A - West	36	55	Age, many wide cracks, lack of treatment	53
A - 17	48	30	Age, surface bleeding	38

It should also be noted that until there are readily available artificial intelligence and machine learning techniques to classify and quantify the distress automatically, the PCI assessments using UAVs will be time consuming because of the vast areas of airport assets and the type of extraneous background noise encountered on these surfaces. Considering all the above information, UAVs are expected to be used as a supplemental data collection tool at airports that require in-depth surface condition assessments. Nevertheless, UAVs have great potential to be used as a data collection tool for other airport applications such as airspace obstruction identification near runway approach zones.

Conclusion

In this study, a non-towered airport was inspected by both traditional and UAV inspections for making condition assessments of various airport surfaces. It is necessary to properly understand the cause of distress before proposing appropriate preventive maintenance techniques to extend the life and reduce the life cycle cost of the airport asset. This study highlights the need to conduct proactive monitoring and preventive maintenance of airport assets. Although this approach intermittently incurs costs, it saves money in the long run and more importantly keeps the airport open compared with a reactive approach where the asset is used until it needs to be completely replaced. Reconstruction of an airport asset will affect the activities of the airport and the associated revenue. Therefore, frequent monitoring will avoid longer downtime of airport assets.

The assessments obtained from both traditional and UAV-based methods were used to estimate the PCI of each airport asset and it is observed that they both classified most of the airport assets under similar condition categories. However, the disagreement percentage provides an idea about the difference in condition assessments and the contributing factors. One such factor is the ability of UAV-based inspections to depict the existing conditions of the airport asset, resulting in greater extents of various distresses. This can be attributed to the 3D models from UAV imagery facilitating the accurate measurement of distress features in a digital environment compared with a traditional visual inspection in the field.

As the current traditional practices are capable of delivering condition assessment information, and the artificial intelligence techniques are not readily available

to automatically classify the distress on 3D models, the application of UAVs can be dedicated to the inspection of high-priority airport assets that require comprehensive surface condition assessments of the whole area. Nevertheless, UAVs have an advantage over traditional inspections while evaluating other airport issues such as airspace intrusions around runway approach zones by fixed objects.

Some recommendations for the application of UAVs for airport inspections include the following. (i) Pilots of crewed aircraft can be informed about the necessity to announce aircraft maneuvers, especially before landing, while UAV inspections of airport assets are going on. This will result in the efficient and safe performance of an aerial inspection of airport assets. (2) Drone RPIC can listen to the CTAF while conducting the airport inspections. (3) Drone RPIC can share the advertisement brochure of the inspections with the airport managers and safety officers for circulation among the airport users. All the stakeholders can be well informed to be supportive of these technologies for safe data collection and inspection.

Acknowledgments

The authors would like to thank the Texas Department of Transportation (TxDOT) for funding project 409877-00001 and other TxDOT personnel who were present during the aerial data collection. The authors acknowledge the NSF Industry-University Cooperative Research Center (I/UCRC) program-funded Center for Integration of Composites into Infrastructure (CICI) site at Texas A&M University (Program Director: Dr. Prakash Balan, Division of Industrial Innovation & Partnerships; Award # 2017796). The authors also acknowledge the support of Hiramani Chimauriya, Amit Gajurel, Kamron Jafari, Dr. Jeff Borowiec, Chris Sasser, Dr. Stacey Lyle, and Brad Hall of the Texas A&M University, as well as Barry Lightfoot and his crew for their assistance during the aerial inspection operations. The support of the RELLIS campus, Texas Virtual Data Library (Texas ViDaL), and High Performance Research Computing (HPRC) facility at Texas A&M University is also gratefully acknowledged.

Author Contributions

The authors confirm contribution to this paper as follows: study conception and design: S. S. C. Congress, A. J. Puppala, C. Treybig, C. Gurganus; data collection: S. S. C. Congress, C. Treybig, J. Halley; analysis and interpretation of results: S. S. C. Congress, A. J. Puppala, C. Treybig, C. Gurganus, J. Halley; draft manuscript preparation: S. S. C. Congress, A. J. Puppala, C. Treybig, C. Gurganus, J. Halley. All authors reviewed the results and approved the final version of the manuscript.

Declaration of Conflicting Interests

The author(s) declared no potential conflicts of interest with respect to the research, authorship, and/or publication of this article.

Funding

The author(s) disclosed receipt of the following financial support for the research, authorship, and/or publication of this article: Texas Department of Transportation project 409877-00001.

ORCID iDs

Surya Sarat Chandra Congress https://orcid.org/0000-0001-5921-9582
Anand J. Puppala https://orcid.org/0000-0003-0435-6285
Charles Gurganus https://orcid.org/0000-0002-6151-1328

Data Accessibility Statement

Some or all data, models, or code that support the findings of this study are available from the corresponding author on reasonable request.

References

1. ASCE. *America's Infrastructure Report Card 2021*. American Society of Civil Engineers, 2021. https://infrastructurereportcard.org/. Accessed March 6, 2021.
2. Colomina, I., and P. Molina. Unmanned Aerial Systems for Photogrammetry and Remote Sensing: A Review. *ISPRS Journal of Photogrammetry and Remote Sensing*, Vol. 92, 2014, pp. 79-97.
3. Siebert, S., and J. Teizer. Mobile 3D Mapping for Surveying Earthwork Projects Using an Unmanned Aerial Vehicle (UAV) System. *Automation in Construction*, Vol. 41, 2014, pp. 1–14.
4. Congress, S. S. C., and A. J. Puppala. Geotechnical Slope Stability and Rockfall Debris Related Safety Assessments of Rock Cuts Adjacent to a Rail Track Using Aerial Photogrammetry Data Analysis. *Transportation Geotechnics*, Vol. 30, 2021, p. 100595.
5. McGlone, J. C., E. M. Mikhail, J. S. Bethel, and R. Mullen. *Manual of Photogrammetry*. American Society for Photogrammetry and Remote Sensing, Bethesda, MD, 2004.
6. Mikhail, E. M., J.S. Bethel, and J. C. Mc Glone. *Introduction to Modern Photogrammetry*. Wiley: New York, 2001.
7. Gonçalves, J. A., and R. Henriques. UAV Photogrammetry for Topographic Monitoring of Coastal Areas. *ISPRS Journal of Photogrammetry and Remote Sensing*, Vol. 104, 2015, pp. 101–111.
8. TxDOT. *Routine Airport Maintenance Program (RAMP) Grants*. Texas Department of Transportation, 2021. http://www.txdot.gov/inside-txdot/division/aviation/airport-grants.html. Accessed May 26, 2021.
9. TxDOT. *Transit Systems Routine Airport Maintenance Program (RAMP) Guidebook*. Texas Department of Transportation, 2013. https://ftp.txdot.gov/pub/txdot-info/d/ramp_coordinator_guidebook.pdf. Accessed May 26, 2021.
10. Walker, D., L. Entine, and S. Kummer. *Advisory Circular 150/5320-17A, Airfield Pavement Surface Evaluation and Rating Manual: Appendix A*. Federal Aviation

Administration, 2014. https://www.faa.gov/documentLibrary/media/Advisory_Circular/150-5320-17a-appendix-a.pdf. Accessed April 30, 2021.
11. ASTM D5340. *Standard Test Method for Airport Pavement Condition Index Surveys*. American Society for Testing and Materials, West Conshohocken, PA, 2020.
12. FAA. *AC 150/5380-7B: Airport Pavement Management*. Federal Aviation Administration, 2014. http://www.faa.gov/airports/resources/advisory_circulars/. Accessed May 26, 2021.
13. FAA. *AC 150/5370-11B - Use of Nondestructive Testing in the Evaluation of Airport Pavements*. Federal Aviation Administration, 2011. https://www.faa.gov/airports/resources/advisory_circulars/index.cfm/go/document.current/documentnumber/150_5370-11. Accessed July 7, 2021.
14. Moreu, F., and M. R. Taha. *Railroad Bridge Inspections for Maintenance and Replacement Prioritization Using Unmanned Aerial Vehicles (UAVs) With Laser Scanning Capabilities*. Rail Safety IDEA Project 32. IDEA, 2018. https://www.trb.org/Main/Blurbs/177995.aspx.
15. Wells, J., and B. Lovelace. *Unmanned Aircraft System Bridge Inspection Demonstration Project Phase II Final Report*. Minnesota Department of Transportation, Research Services & Library, St Paul, 2017.
16. Neubauer, K., E. Bullard, and R. Blunt. *Collection of Data With Unmanned Aerial Systems (UAS) for Bridge Inspection and Construction Inspection*. Federal Highway Administration, Office of Infrastructure, McLean, VA, 2021.
17. McCormack, E., and J. Stimberis. Small Unmanned Aircraft Evaluated for Avalanche Control. *Transportation Research Record: Journal of the Transportation Research Board*, 2010. 2169: 168–173.
18. Bullock, J. L., R. Hainje, A. Habib, D. Horton, and D. M. Bullock. Public Safety Implementation of Unmanned Aerial Systems for Photogrammetric Mapping of Crash Scenes. *Transportation Research Record: Journal of the Transportation Research Board*, 2019. 2673: 567–574.
19. Hainen, A. M., A. L. Stevens, C. M. Day, H. Li, J. Mackey, M. Luker, M. Taylor, J. R. Sturdevant, and D. M. Bullock. High-Resolution Controller Data Performance Measures for Optimizing Diverging Diamond Interchanges and Outcome Assessment With Drone Video. *Transportation Research Record: Journal of the Transportation Research Board*, 2015. 2487: 31–43.
20. Congress, S. S. C., A. J. Puppala, P. Kumar, A. Banerjee, and U. D. Patil. Methodology for Resloping of Rock Slope Using 3D Models From UAV-CRP Technology. *ASCE Journal of Geotechnical and Geoenvironmental Engineering*, Vol. 147, No. 9, 2021, P. 05021005. https://doi.org/10.1061/(ASCE)GT.1943-5606.0002591.
21. Congress, S. S. C., A.J. Puppala, and C. L. Lundberg. Total System Error Analysis of UAV-CRP Technology for Monitoring Transportation Infrastructure Assets. *Engineering Geology*, Vol. 247, 2018, pp. 104–116. https://doi.org/10.1016/j.enggeo.2018.11.002.
22. Lin, Y., and S. Saripalli. Road Detection and Tracking From Aerial Desert Imagery. *Journal of Intelligent & Robotic Systems*, Vol. 65, No. 1–4, 2012, pp. 345–359.
23. Ham, Y., K. K. Han, J. J. Lin, and M. Golparvar-Fard. Visual Monitoring of Civil Infrastructure Systems via Camera-Equipped Unmanned Aerial Vehicles (UAVs): A Review of Related Works. *Visualization in Engineering*, Vol. 4, No. 1, 2016, p. 1.
24. Congress, S. S. C., A. J. Puppala, M. D. A. Khan, and N. Biswas. *TRB Centennial Circular: Application of Unmanned Aerial Technologies for Inspecting Pavement and Bridge Infrastructure Asset Condition*. Transportation Research Board, Washington, D.C., 2020, p. 134.
25. Kim, S., D. Paes, K. Lee, J. Irizarry, and E. N. Johnson. UAS-Based Airport Maintenance Inspections: Lessons Learned From Pilot Study Implementation. In *Computing in Civil Engineering 2019: Smart Cities, Sustainability, and Resilience* (Y. K. Cho, F. Leite, A. Behzadan, and C. Wang eds.), American Society of Civil Engineers, Reston, VA, 2019, pp. 382–389.
26. Booz Allen Hamilton, Embry-Riddle Aeronautical University, Hogan Lovells, Kimley-Horn and Associates, Novel Engineering, Toltz King, Duvall, Anderson Associates, Vanasse Hangen Brustlin, Inc., and Astrid Aviation and Aerospace. *Airports and Unmanned Aircraft Systems, Volume 3: Potential Use of UAS by Airport Operators*. The National Academies Press, Washington, D.C., 2020.
27. Congress, S. S. C., A. J. Puppala, A. Gajurel, and N. H. Jafari. Transforming Aerial Reconnaissance Data of Pavement Infrastructure Into Knowledge for Better Response to Natural Disasters. In *Geo-Extreme 2021* (C. L. Meehan, M. A. Pando, B. A. Leshchinsky, and N. H. Jafari, eds.), American Society of Civil Engineers, Reston, VA, 2021, pp. 183–193.